Electric Vehicle Transportation Center

Cell Emulation and Preliminary Results

Matthieu Dubarry and Arnaud Devie
Hawaii Natural Energy Institute
University of Hawaii at Manoa
1680 East West Road, POST 109
Honolulu, HI 96822
E-mail: matthieu@hawaii.edu

Submitted to:

Dr. David Block
Florida Solar Energy Center
University of Central Florida
1679 Clearlake Road
Cocoa, FL 32922
E-mail: block@fsec.ucf.edu

Purchase Order Number: 291166
Report Number: HI-11-16
July 2016

HNEI
Hawai'i Natural Energy Institute
School of Ocean and Earth Science and Technology
University of Hawai'i at Mānoa

University of Central Florida

Cell Emulation and Preliminary Results

Hawaii Natural Energy Institute

July 2016

I. Abstract

This report details preliminary results of the testing plan implemented by the Hawaii Natural Energy Institute to evaluate Electric Vehicle (EV) battery durability and reliability under electric utility grid operations. Commercial EV battery cells are tested in order to assess the impact of vehicle to grid and grid to vehicle applications on cell degradation. The plan also includes testing other usages associated with EVs under grid operations such as the impact of charging level and charging habits. This report first details the procedure used to analyze the electrochemical behavior of the cells and then provides an update on the testing status as well as preliminary visualization of the data gathered so far.

II. Introduction

In the previous report [1], a test plan based on the application of design of experiments techniques for both the cycling and the calendar aging study was proposed. Following this plan, the impact of vehicle to grid (V2G) and grid to vehicle (G2V) strategies as well as the impact of charging habits on lithium-ion (Li-ion) cells can be assessed. In a second report, the implementation of the initial conditioning and characterization test (ICCT) phase [2] was presented. The cycle aging experiments and the calendar aging experiments have been running for about 6 months and now is the time to start looking into the battery degradation associated with the different aging conditions.

Battery degradation is influenced by many factors, either at the single cell level or at the assembly level, and their effects are often inter-related. As the system is being scaled up from single cells to modules and packs, the number of stress factors increases and their interdependence intensifies.

At the single cell level, degradation factors have thermodynamics and kinetics origins. The variations of these properties are affected by the environment (e.g., temperature or pressure) and duty cycle (e.g., voltage, rate) [3-6]. At the assembly level, additional factors need to be considered with a large number of cells in a topological arrangement. For instance, cell quality and its variability, presence of an internal temperature gradient or heat distribution and imbalance among the cells are all critical considerations in battery management systems (BMS) [7, 8]. Other factors include contact resistance variation with time and vibration or corrosion. The imbalance issue and quantifying the effect on performance of a battery assembly are currently under investigation in other projects in the Hawaii Natural Energy Institute laboratory [7, 8], along with a recently published study on how to properly define and estimate the state of charge (SOC) from a cell to a battery pack[9].

One of the most critical aspects in applying practical diagnostics and prognostics tools is the ability to categorize and quantify contributions from different attributes of the degradation processes [3-5]. Unfortunately, most of the observations are typically obtained from post-mortem physical measurements or characterization techniques that are cost prohibitive to implement or just inadequate for online diagnostics and prognostics.

Readily available electrical measurements remain the most cost effective method to monitor the battery condition. Analyzing the voltage, current, and temperature of the battery is feasible within the BMS. Online diagnostics and prognostics will then be possible if the degradation mechanism can be deciphered from those measurements. In recent years in other studies, online diagnostics and prognostics have been shown to be possible [6, 10, 11] and that every degradation mechanism could belong to at least one of three categories of attributes to degradation. These attributes are: (1) loss of active materials, (2) loss of lithium inventory, and (3) change in reaction kinetics. Using such simple classifications, allows for translation of qualitative degradation phenomena into quantifiable contributions from the three categories of degradation.

Two methods are instrumental in achieving this quantification: one is tracking the SOC of the cell using the Open Circuit Voltage (OCV) measurements [12], the other is tracking the state of health (SOH) using the incremental capacity (IC) dQ/dV analysis [6, 10, 11]. This derivative technique looks at the evolution of the increments of capacity (dQ) per increment of voltage (dV). To facilitate dQ/dV analysis, a model to emulate degradation losses based on the attributes [6] was developed. Such a capability enables handling of the aging-pathway dependence with great flexibility. This report first describes the methodology that will be used to analyze the results of the experiments. A more complete description of our approach can be found in [13] an open source format. Additionally, preliminary results are presented on the cycle aging and of the calendar aging experiments described in the previous reports.

III. Cell Emulation

To understand the capacity fading mechanism and for reliable cell by cell diagnosis, a detailed analyses using an in-house incremental capacity (dQ/dV) technique was conducted. Detailed descriptions of this technique are reported in Refs [6, 10, 11].

III.1 Methodology

In the incremental capacity technique approach, the starting hypothesis is that in most cases, although the cell is degrading, but the electrochemical behavior of each individual electrode is not changing significantly. The capacity loss is then induced by either a change in the electrode balance (a loss of active material on either side) or a change in the amount of lithium ions that could go back and forth between the electrodes. More precisely, the low current capacity fade of any lithium-ion cell can then be attributed to at least one of five degradation modes: loss of lithium inventory (LLI), loss of active material (LAM) in a lithiated (li) or delithiated (de) state at the positive electrode (PE) or negative electrode (NE) (as denoted by LAM_{dePE}, LAM_{liPE}, LAM_{deNE}, and LAM_{liNE}, respectively).

Any change in electrode balance and/or lithium content will modify the voltage response of the battery. Therefore studying the changes in the voltage curve upon aging will provide an insight on the degradation pattern of any cell. As the variations can be pretty minute, they are better noticed by looking at a derivative of the voltage curve: dQ/dV. An example of the incremental capacity signature is presented in Figure 1 for a graphite/ $LiNi_xAl_yCo_{1-x-y}O_2$ (NCA), which is assumed to be the chemistry of the Panasonic cells selected for this research.

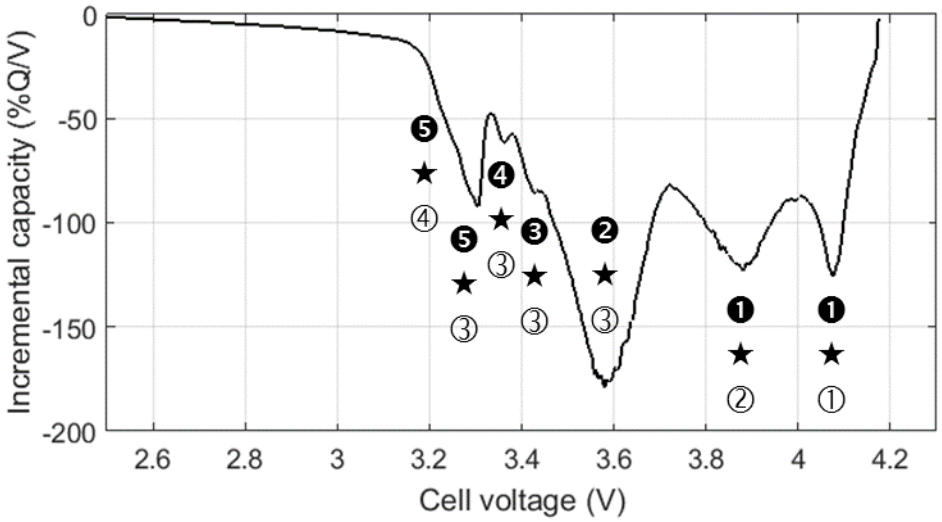

Figure 1: Example of the incremental capacity signature of a G//NCA cell.

The couples {❶★⓪} in Figure 1 refer to the different electrochemical reactions occurring at each electrodes. The black circles represent the reaction number in the negative electrode (NE) and the white circles the reaction number in the positive electrode (PE). Each peak on the incremental capacity curve then corresponds to the convolution of reactions in both electrodes, i.e. that the shape of each peak is influenced by both electrodes. Studying their evolution with aging will provide a precise understanding of the degradation mechanisms.

Unfortunately, the deconvolution of the influence of the PE and NE can be tricky. A graphical analogy can be used in order to facilitate the comprehension of the convolution of reactions in each electrode: to imagine the battery as a clepsydra, i.e., a water clock, with two connected bulbs filled with a liquid. In this analogy, as displayed in Figure 2, each electrode is represented by its incremental capacity curve vs. a reference electrode. The two IC curves serve as the bulbs in the clepsydra and the amount of liquid held in the clock (the yellow area) serves as a representation of the lithium inventory. The upper bulb represents the NE and the lower one the PE. When the battery is discharging, the lithium ions flow from the NE to the PE; thus, in the clepsydra analogy, the yellow area in the upper bulb is decreasing while increasing in the lower bulb. The cell voltage is proportional to the difference in the liquid levels between the two bulbs.

Using this illustration, each peak in the incremental capacity curve can be indexed from the individual electrode IC curves by looking at the liquid level in each bulb while the charge or discharge progresses. This is exemplified by the three different schematics in Figure 2.

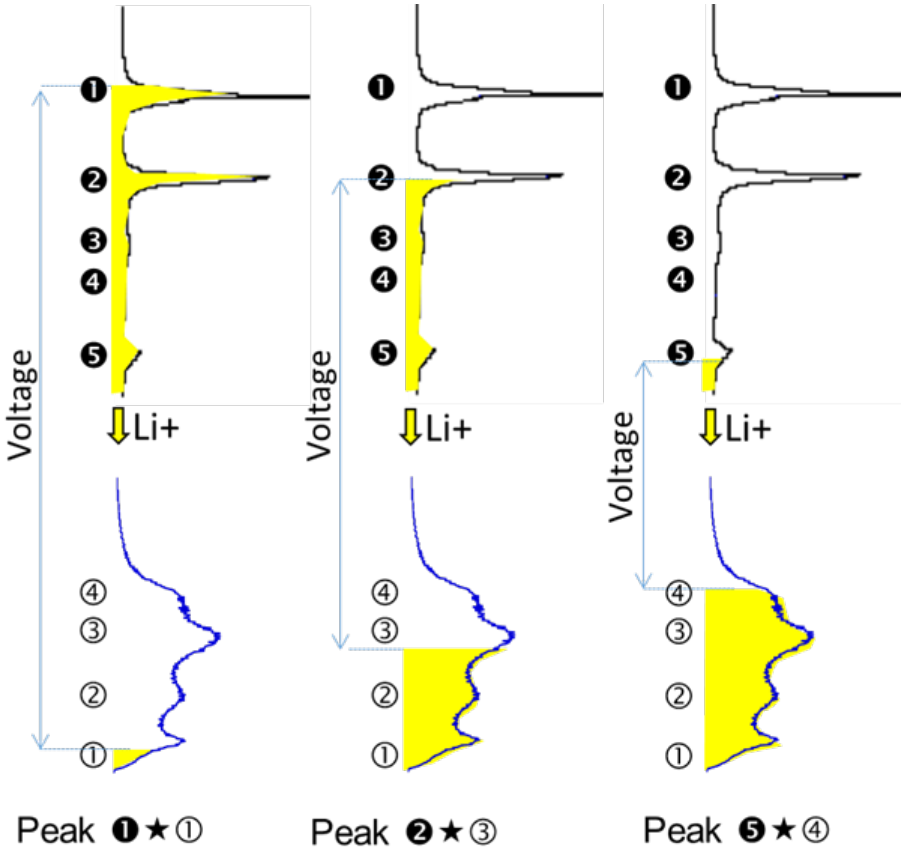

Figure 2: Peak indexation using the clepsydra analogy during discharge.

Keeping the clepsydra analogy, the effects of most degradation mechanisms on the incremental capacity curves [13], shown in Figure 3. For a simple case involving cell impedance change, a smaller separation of the two bulbs (light blue frame) is created. Deteriorating kinetics broaden the peaks (blue frame). For LLI and LAM, there is more complicated alterations in the IC curves. In the case of LAM on one of the electrodes, the associated bulb becomes smaller, so the rate of filling/emptying the peaks will increase (red frame). In the case of LLI, the bulbs size remains the same, but the amount of available lithium ions is lowered in the upper bulb (yellow frame). This action is like a leak in the clepsydra, the total yellow area in the bulbs is then diminished.

Using this process, changes in the incremental capacity signature to one of the degradation categories can be associated without an in-depth understanding of the underlying electrochemical reactions. However, this graphical method suffers from some limitations; although qualitative and quantitative information are decipherable, it could be time consuming and it also lacks the ability to define protocols to fully analyze the data in a systematic manner.

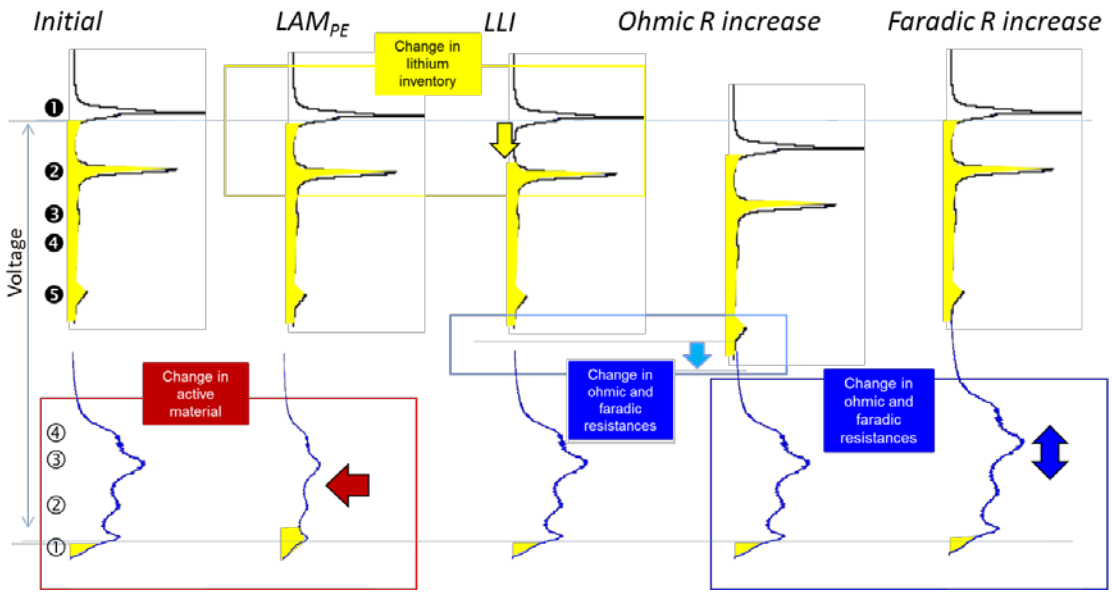

Figure 3: Illustration of the effect of different degradation mechanisms on the incremental capacity curves.

Our in-house model [6], named *'alawa* for the Hawaiian word for "to diagnose", circumvents these issues and operates by emulating the full cell behavior from half-cell (positive and negative electrode active materials) test data. This test data is harvested from the cells themselves or collected from the materials provided by manufacturers or other commercial sources. In other words, it allows playing with the clepsydra bulbs size and content and, thus, deriving the changes in voltage response and capacity retention.

III.2 Half-cell results

For this study, and to improve accuracy, electrode materials from cell #103 were harvested and then characterized individually versus a lithium reference electrode (this is referred as half-cell testing). In order to be safely disassembled, cell 103 was first fully discharged to 2V using a CCCV technique with a C/200 limiting current (discharge in 200 hours). After completion of the discharge, the cell was entered in an argon-filled glove box for disassembly. Once in place, a pipe cutter was used to cut both end caps and a rotary tool equipped with a diamond coated cutting disc was used to cut a straight line in the central cylinder freeing the "jelly roll" of electrodes (Figure 4a and b). Commercial electrodes are usually double sided and for the electrochemical tests, the active material layer on one side of each the electrode must be removed. The one-side active material was removed by gently rubbing the electrodes with a solvent soaked cotton tip. To avoid solvent seepage to the other side on which the electrochemical measurements are to be made, solvent was applied only to the inner section of the side to be removed. The edges remained untouched to the solvent. Moreover, to decrease further the risk of electrode contamination from the disassembling process, the electrodes (0.71 cm^2) were punched near the center of the electrode roll. Thereafter, in order to extract the lithium salt, the electrodes were rinsed in fresh dimethyl carbonate (DMC).

Electrochemical analyses were performed in Swagelok type cells (1/2" PTFE-type, Figure 4c) with a lithium metal-coated stainless steel disk as counter electrode and two layers of Whattman GF/D borosilicate glass fiber disk as separator. The electrolyte consisted of a 1 $mol.L^{-1}$ of LiPF6 in 1:1 (by weight) EC/DMC solution with 2%$_{wt}$ Vinylene Carbonate (VC) additive.

III.2.1 Conditioning cycles

Electrochemical measurements were carried out using a potentiostat from Bio-Logic (VMP3), Figure 4d. The Swagelok cells underwent conditioning and reference performance testing (RPT). The positive electrode was cycled from 4.35 V to 3.0 V. Its conditioning cycles consisted of a 1 charge/discharge cycle at a C/45 rate, followed by 6 cycles at a C/3.5 rate. The graphite intercalation compound (GIC) electrode was cycled from 0.01 V to 1.8 V, and its conditioning consisted of 1 cycle at a C/30 rate followed by 5 cycles at a C/25 rate. These conditioning cycles on both electrodes were followed by a reference performance test (RPT) that consisted of a series of charge/discharge cycle at different rates: C/40, C/20, C/10, C/5, C/2 and C/1.

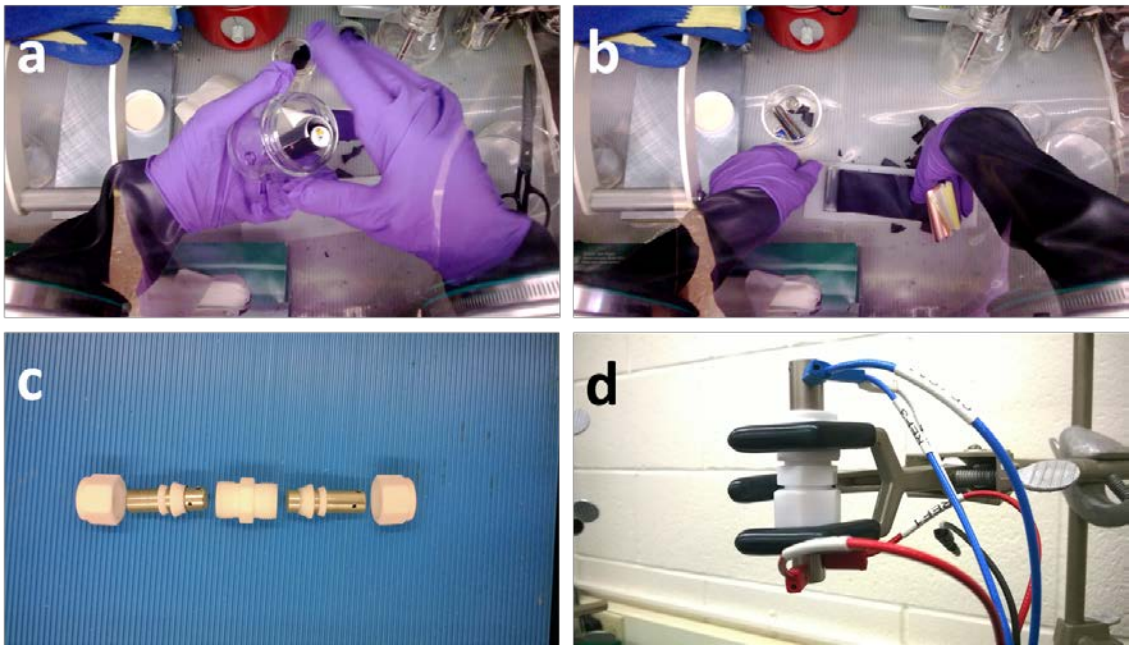

Figure 4: (a&b) cell jelly roll, (c) swagelock type cell and (d) Swagelok cell connected to a battery tester.

The conditioning cycles serve two purposes: estimating the electrode balance and making sure that the electrode material is stable prior to performing the RPT. The first cycle of a Li-ion cell is often linked with a large capacity loss, on the order of 10%. This loss is commonly associated with the formation of a solid electrolyte interphase (SEI) layer at the surface of the negative electrode. The same thing can also happen on the positive electrode to a lesser degree. These SEI layers are usually completely formed when the cells leave the manufacturing plant but the washing with DMC performed during the electrode preparation phase is known to dissolve this thin layer. Therefore the first cycles of the half-cells will show a significant capacity loss that could give information about the extent of the loss that occurred in the full cells. In any case, a few cycles are necessary to stabilize the electrode prior to the reference performance test.

III.2.2 Reference Performance tests

Figure 5 presents the results of the reference performance test for the positive electrode. Figure 5(a) showcases the traditional voltage vs. capacity curves highlighting the changes in electrochemical response with the increase of the current. The more current is passed in the cell, the less capacity is available and the more polarization is present. E.g., at C/1, the positive electrode only delivers around 60% of the low rate capacity and it presents a 400mV higher

polarization. Figure 5(b) presents the IC derivative of the data in Figure 5(a). In this representation, the capacity increments per voltage increments, dQ/dV, are plotted as a function of the cell voltage.

The IC signature of the positive electrode is compatible with literature data on the $LiNi_xAl_yCo_{1-x-y}O_2$ (NCA) chemistry. There are some kinetic limitations towards the end of charge and end of discharge. This induces a great asymmetry between the charge and discharge curves at low and high voltages. There is also an energy activation barrier to start the charging process (removing Li-ions from the structure), this explains the shape and the intensity of the low voltage peak in charge.

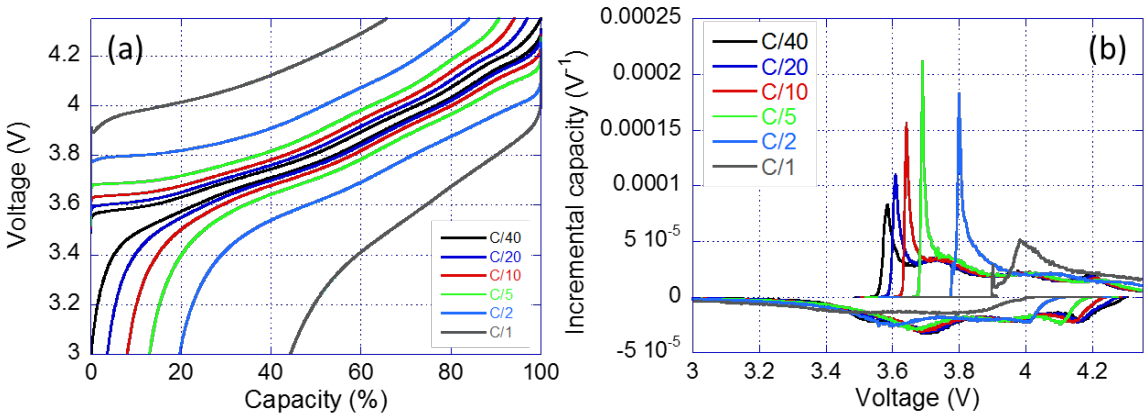

Figure 5: RPT results for the positive electrode. (a) V vs.Q curves and (b) associated incremental capacity signature.

Figure 6 presents the same figure for the negative electrode. The IC signature of the negative electrode is compatible with literature data on the C_6 (graphite, G) chemistry.

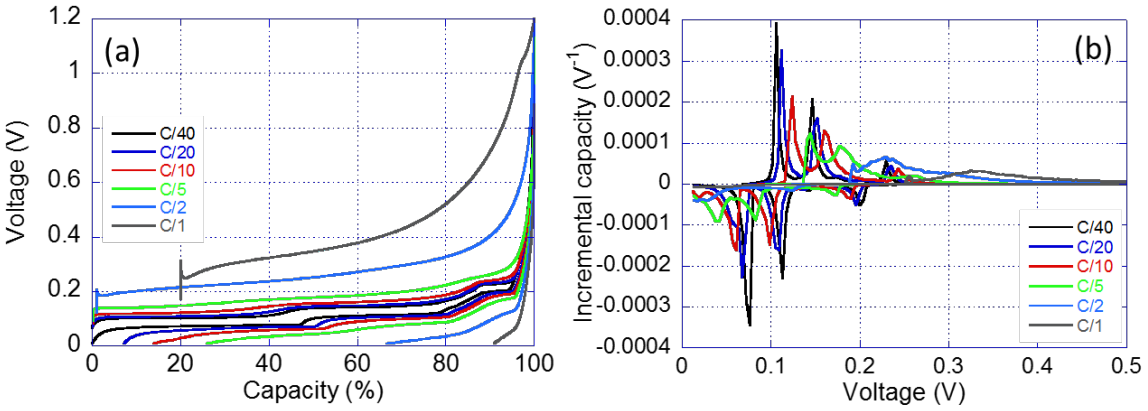

Figure 6: RPT results for the negative electrode. (a) V vs.Q curves and (b) associated incremental capacity signature.

III.2.3 Cell Emulation

The RPT data was imported in the *'alawa* toolbox [14] in order to be able to emulate the full cell behavior from the half-cell data [6, 13]. The matching of the electrodes depends mainly on 2 parameters: the initial loading ratio and offset. The loading ratio (LR) corresponds to the capacity ratio between the two electrodes, i.e., the size of the bulbs relative to one another. The offset (OFS) correspond to the shift between the electrodes induced during the formation of the cell (initial SEI growth and/or irreversible material loss during the first few cycles), i.e., the

quantity of liquid spilled out when filling the clepsydra. Figure 7(a) illustrate the definition of the LR and the OFS and Figure 7(b) shows the results of the emulation. The LR was estimated at 0.96, the OFS to 2.8%. Since the half-cell data was collected using different electrolyte and separators than of the one used in the full cell, some additional minor adjustments were necessary in order to yield a better fit: the resistance was compensated by 0.3 Ω and the electrodes kinetics were accelerated by a factor 2. With cell emulation successful, confidence was obtained on the ability to diagnose the cell degradation. Such analysis will be presented in upcoming reports.

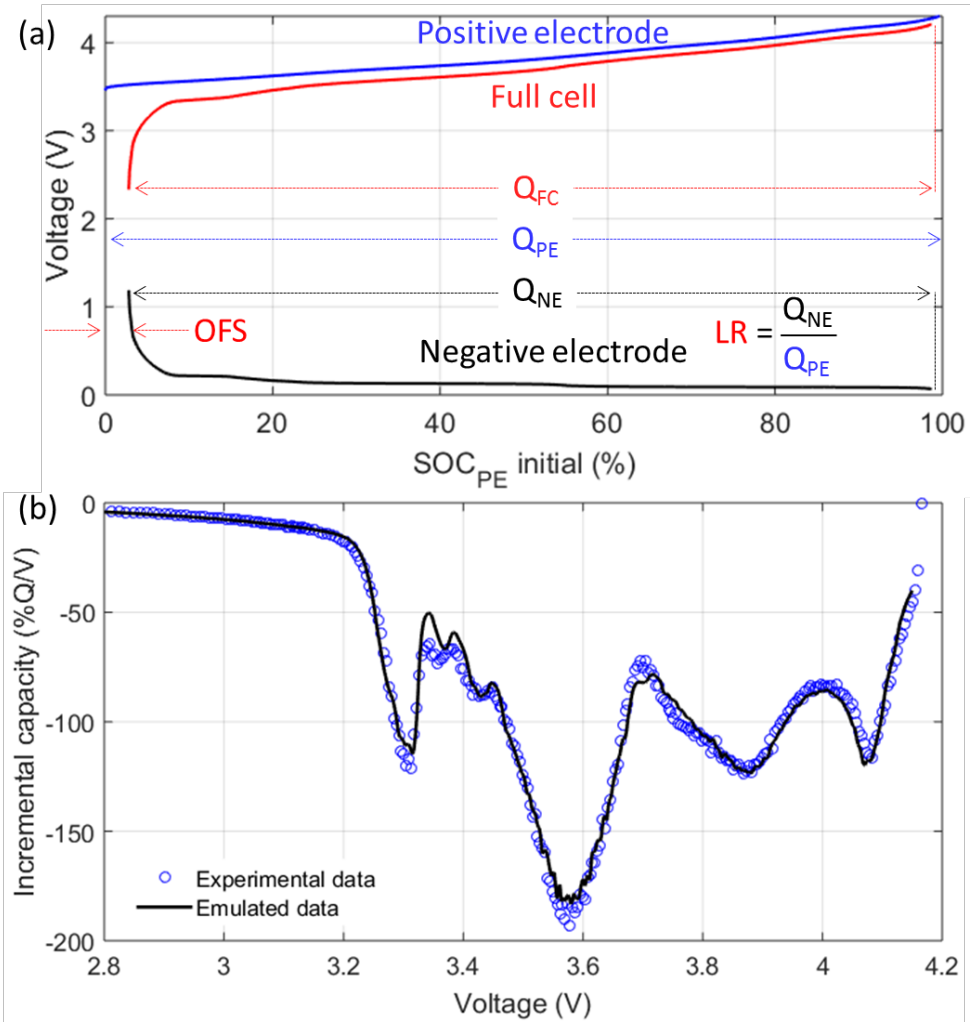

Figure 7:(a) Cell architecture emulated in the 'alawa toolbox and (b) comparison of the IC curves of the experimental and emulated cells at a C/33 rate.

IV. Preliminary testing results

IV.1 Cycle aging

IV.1.1 Testing implementation

Figure 8 presents details on the 12 schedules used in this study (additional information can be found in [1]) and Figure 9 shows the exchanged capacity for each schedule. The most aggressive

schedule, the one involving V2G episodes at both day and night periods (DCR-DCR [1]), exchanges close to 80% of the battery capacity for each equivalent "day" of cycling. The less aggressive schedules, the ones with no V2G, exchanges about 27% of the cell full capacity. As expected from the calculations in our previous reports [1, 2], the V2G step uses about 25% of the cell capacity whereas the driving step uses about 27% of the cell capacity.

In terms of depth of discharge (DOD), the smallest usage of the cells corresponds to the schedules with no V2G and a charge during period 1 (CR and RC schedules). In those, the DOD on the cells is no more than 13.5% before the cell is recharged. The highest DOD corresponds to the schedule with a rest in period 1 and a V2G step in the 2nd period (R-DCR). In this schedule the DOD comes to about 52% when the charge is starting (27% from both driving schedules and 25% from the V2G step).

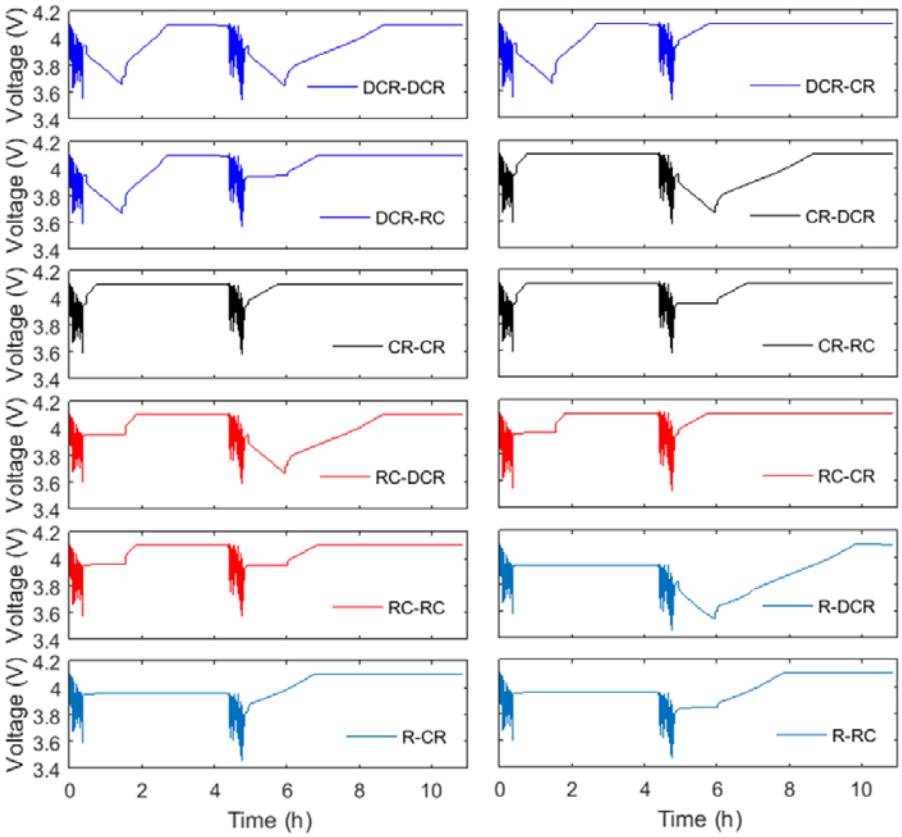

Figure 8: Details on the 12 schedules used in this study.

[1] D: discharge (V2G), C: charge (G2V), R: rest (idle)

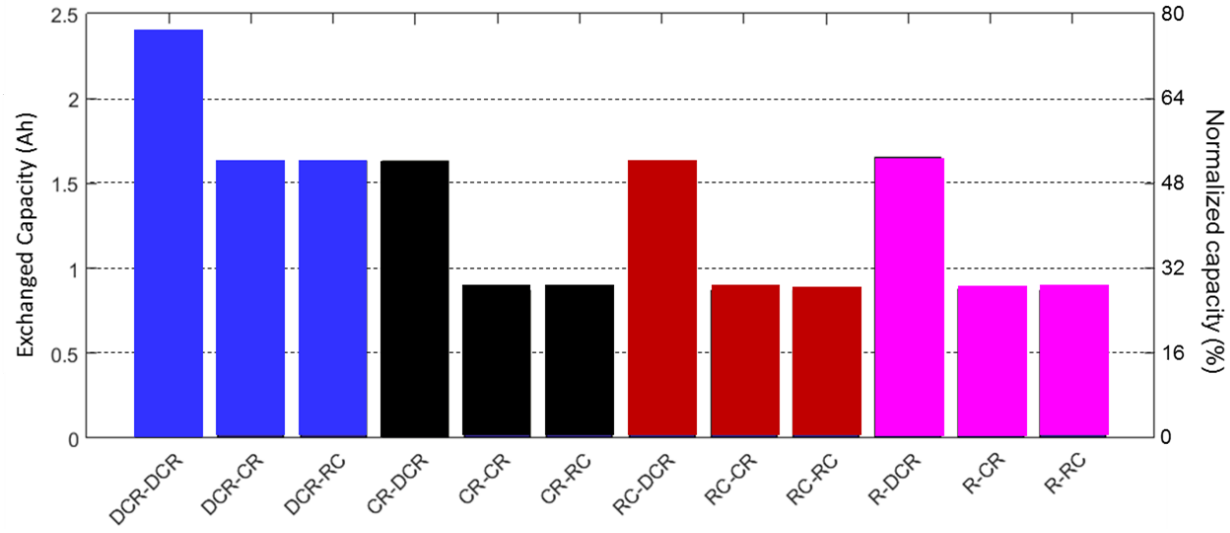

Figure 9: Exchanged capacity for each schedule.

IV.1.2 Degradation summary after 3 equivalent trimesters of testing

As described in [1, 2], the schedules presented in the previous section last 11 hours. The schedules are repeated 24/7 for 6 weeks before a reference performance test is performed in order to check on the cell degradation. During those 6 weeks, the schedules are repeated 90 times and since they account for 1 equivalent day, the reference performance tests are spread by 90 "days" which corresponds to a quarter of a year. Figure 10 presents the observed capacity loss for the first 3 equivalent trimesters. Over these 270 equivalent days of testing, the cells lost between 3.5 and 6% capacity. Figure 11 presents the capacity loss after three quarters as a function of the schedule. As can be seen, there is a clear impact of the V2G implementation which always induces more capacity loss (DCR schedules). Interestingly, the schedules with only 1 charge per day (R-*) are degrading faster than the schedules with 2 charges per day. This might be induced by the deeper DOD.

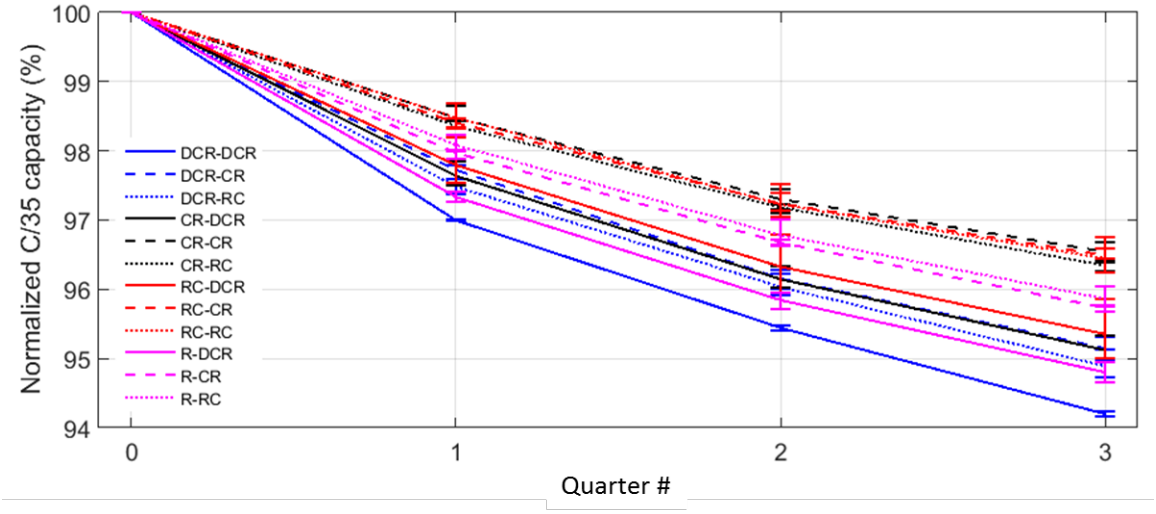

Figure 10: Capacity loss per quarter

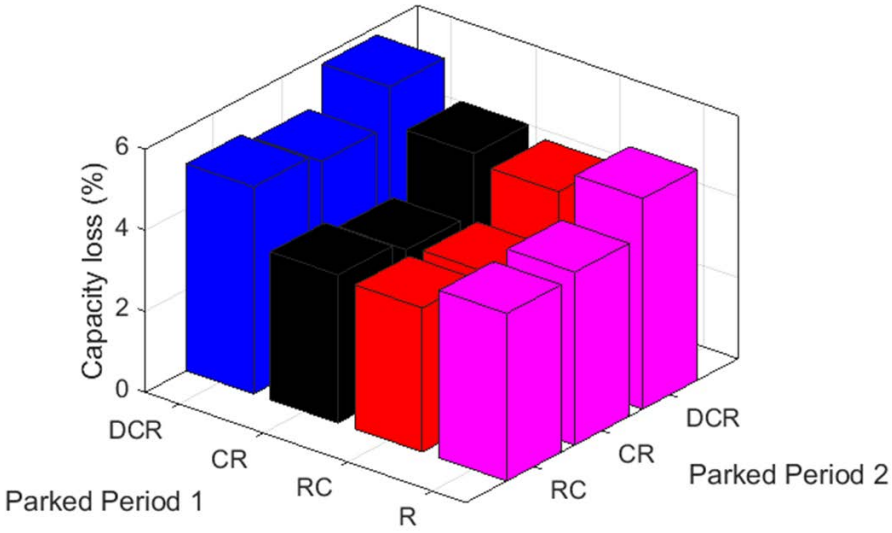

Figure 11: Capacity loss at the 3rd trimester in function of the schedule.

Looking at the changes in voltage response, shown in Figure 12, clear evolution of the curves can be seen. The degradation mechanism is not straight forward and will be discussed in a following report.

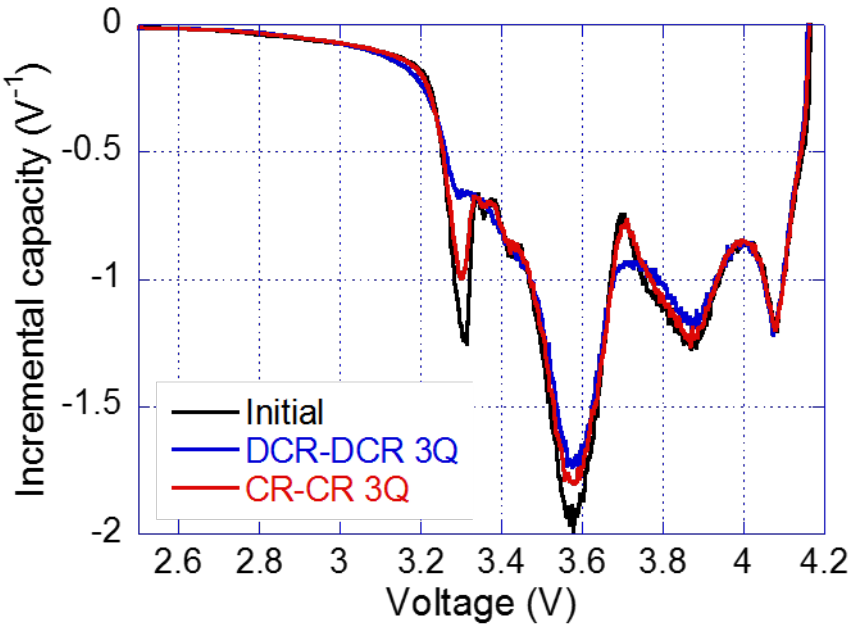

Figure 12: Change in IC curves at the 3rd trimester for the least and most degraded cell compared to the initial curve.

IV.2 Calendar aging

Figure 13(a) presents the capacity loss associated with the first 12 weeks of calendar aging. The chosen temperature and SOC are described in details in [1]. Figure 13(b) showcases the relationship between capacity loss, temperature and SOC. The dotted surface represents the modeled quadratic relationship between the parameters and the contour curves projected on the base corresponds to 0.5% capacity loss increments. The loss observed for high temperature and high SOC is 0.5% capacity per week. At room temperature, storing the cell at high SOC seems to induce a 0.2%/week capacity loss. Storing the cells half charged seems to reduce the loss to 0.15%/week. If these trends continues, the cells could lost 8 - 10% of their capacity yearly just from sitting at room temperature. However, based on experience and literature data, we anticipate the degradation pace to slow down in the coming weeks.

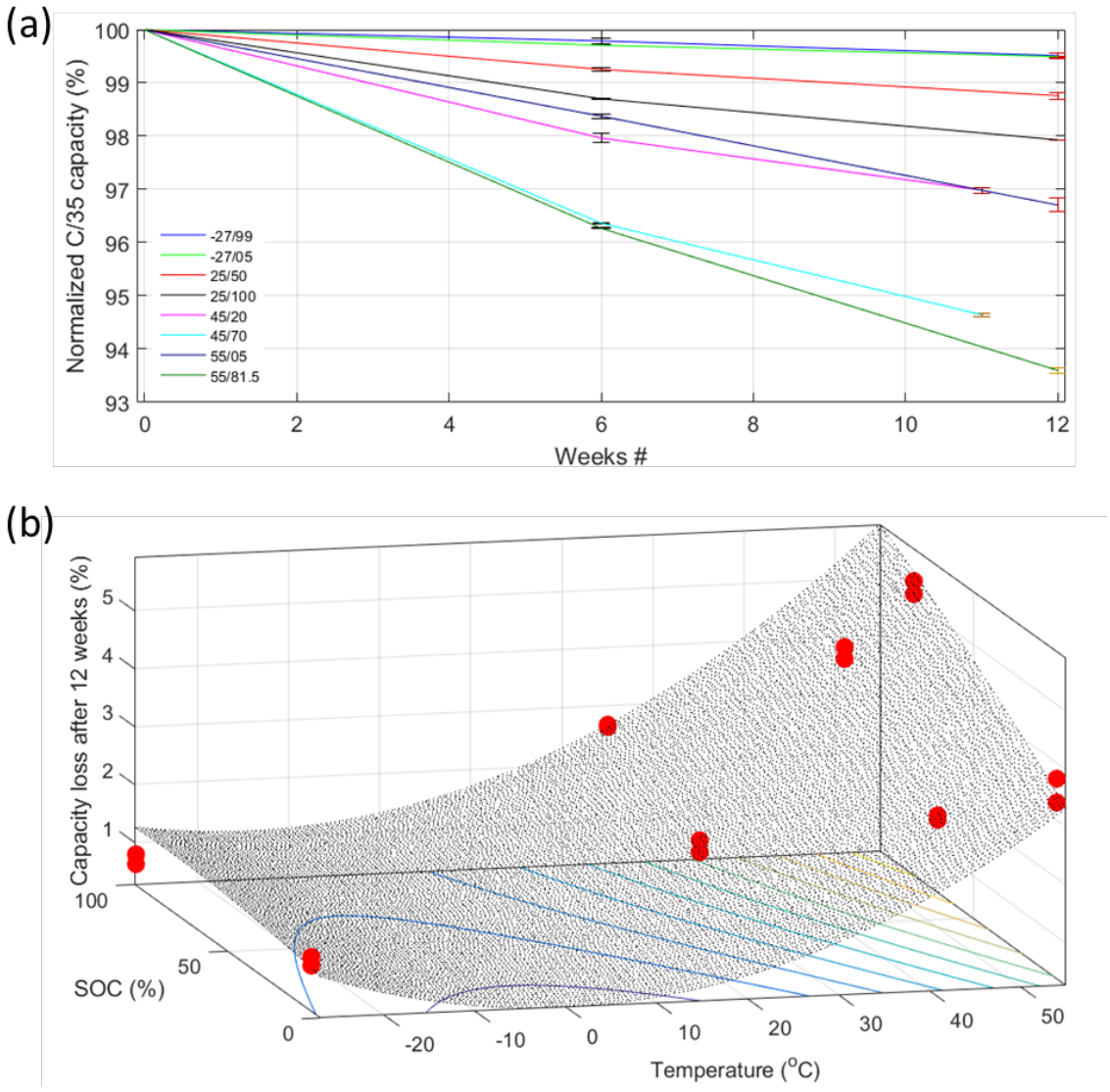

Figure 13: Capacity loss induced by calendar aging. (a) vs. time and (b) vs. temperature and SOC.

IV.3 Test status summary

As of October 31st 2015, the cells performing the cycling experiment were cycled 300 times and are now ready for their fifth reference performance test (RPT). The cells performing calendar aging aged between 14 and 17 weeks. The first set of cells (038, 039, 043 and 044) is set to perform their fourth RPT in the coming week. The detailed test status is presented in Table 1.

Table 1: Test status as of October 31st, 2015.

Main experiment

Cell #	Aging type*	ICCT	As of October 31st 2015 RPT	EQ. Days
NCRB001	DCR-DCR	✓	4	300
NCRB002	DCR-DCR	✓	4	300
NCRB003	DCR-DCR	✓	4	300
NCRB004	DCR-CR	✓	4	300
NCRB005	DCR-CR	✓	4	300
NCRB006	DCR-CR	✓	4	300
NCRB007	DCR-RC	✓	4	300
NCRB008	DCR-RC	✓	4	300
NCRB009	DCR-RC	✓	4	300
NCRB010	CR-DCR	✓	4	300
NCRB011	CR-DCR	✓	4	300
NCRB012	CR-DCR	✓	4	300
NCRB013	CR-CR	✓	4	300
NCRB014	CR-CR	✓	4	300
NCRB015	CR-CR	✓	4	300
NCRB016	CR-RC	✓	4	300
NCRB017	CR-RC	✓	4	300
NCRB018	CR-RC	✓	4	300
NCRB019	RC-DCR	✓	4	300
NCRB020	RC-DCR	✓	4	300
NCRB021	RC-DCR	✓	4	300
NCRB022	RC-CR	✓	4	300
NCRB023	RC-CR	✓	4	300
NCRB024	RC-CR	✓	4	300
NCRB025	RC-RC	✓	4	300
NCRB026	RC-RC	✓	4	300
NCRB027	RC-RC	✓	4	300
NCRB028	R-DCR	✓	4	300
NCRB029	R-DCR	✓	4	300
NCRB030	R-DCR	✓	4	300
NCRB031	R-CR	✓	4	300
NCRB033	R-CR	✓	4	300
NCRB034	R-CR	✓	4	300
NCRB035	R-RC	✓	4	300
NCRB036	R-RC	✓	4	300
NCRB037	R-RC	✓	4	300

Calendar aging

Cell #	Aging type	ICCT	As of October 31st 2015 RPT	AGING
NCRB038	-27°C|99% SOC	✓	3	17 weeks
NCRB039	-27°C|99% SOC	✓	3	17 weeks
NCRB043	-27°C|06% SOC	✓	3	17 weeks
NCRB044	-27°C|06% SOC	✓	3	17 weeks
NCRB046	25°C|50% SOC	✓	3	16 weeks
NCRB047	25°C|50% SOC	✓	3	16 weeks
NCRB049	25°C|100% SOC	✓	3	16 weeks
NCRB050	25°C|100% SOC	✓	3	16 weeks
NCRB056	45°C|20% SOC	✓	3	15 weeks
NCRB058	45°C|20% SOC	✓	3	15 weeks
NCRB059	45°C|70% SOC	✓	3	15 weeks
NCBR063	45°C|70% SOC	✓	3	15 weeks
NCRB069	55°C|81.5% SOC	✓	3	14 weeks
NCRB083	55°C|81.5% SOC	✓	3	14 weeks
NCRB085	55°C|06% SOC	✓	3	14 weeks
NCRB093	55°C|06% SOC	✓	3	14 weeks

*D: P/4 discharge
C: Charge
R: Rest

V. Conclusions

Overall, the proposed testing plan is being followed and trends have started to emerge. Intensive V2G usage (1hour at a quarter of the car maximum power) seems to induce additional capacity loss. Interestingly, it also appears that charging twice a day is beneficial to the cells. Regarding calendar aging, the high temperature and high SOC induced more degradation, more than 5% in 12 weeks, than the lower temperature / SOC combination. The cells stored at -27°C hardly experienced any loss. The cells stored at 25°C experienced a 0.15 to 0.2% loss per week.

VI. Acknowledgements

This report was funded under a sub award to the Hawaii Natural Energy Institute, University of Hawaii at Manoa, from the Florida Solar Energy Center, University of Central Florida, through a grant from the US Department of Transportation's University Transportation Centers Program, Research and Innovative Technology Administration.

VII. References

[1] M. Dubarry, EVTC Report HNEI-03-15, (2015) 1-14.
[2] M. Dubarry, A. Devie, EVTC Report HNEI-06-15, (2015) 1-25.
[3] J. Groot, in: Division of Electric Power Engineering, Chalmers University of Technology, Göteborg, 2014, pp. 112.
[4] M. Broussely, P. Biensan, F. Bonhomme, P. Blanchard, S. Herreyre, K. Nechev, R.J. Staniewicz, J. Power Sources, 146 (2005) 90-96.
[5] J. Vetter, P. Novák, M.R. Wagner, C. Veit, K.C. Möller, J.O. Besenhard, M. Winter, M. Wohlfahrt-Mehrens, C. Vogler, A. Hammouche, J. Power Sources, 147 (2005) 269-281.
[6] M. Dubarry, C. Truchot, B.Y. Liaw, J. Power Sources, 219 (2012) 204-216.
[7] C. Truchot, M. Dubarry, B.Y. Liaw, Appl. Energy, 119 (2014) 218-227.
[8] M. Dubarry, N. Vuillaume, B.Y. Liaw, Int J Energ Res, 34 (2010) 216-231.
[9] M. Dubarry, C. Truchot, A. Devie, B.Y. Liaw, J. Electrochem. Soc., 162 (2015) A877-A884.
[10] A. Devie, M. Dubarry, B.Y. Liaw, J. Electrochem. Soc., 162 (2015) A1033-A1040.
[11] M. Dubarry, C. Truchot, B.Y. Liaw, J. Power Sources, 258 (2014) 408-419.
[12] M. Dubarry, C. Truchot, B.Y. Liaw, K. Gering, S. Sazhin, D. Jamison, C. Michelbacher, J. Power Sources, 196 (2011) 10336-10343.
[13] M. Dubarry, A. Devie, B.Y. Liaw, Journal of Energy and Power Sources, 1 (2014) 242-249.
[14] https://www.soest.hawaii.edu/HNEI/alawa/